Journal of Biomolecular NMR, **26:** 259–275, 2003.
KLUWER/ESCOM

Similarities between intra- and intermolecular hydrogen bonds in RNA kissing complexes found by means of cross-correlated relaxation

Jens Dittmer[a], Chul-Hyun Kim[b] & Geoffrey Bodenhausen[a,c,*]
[a]*Institut de Chimie Moléculaire et Biologique, Ecole Polytechnique Fédérale de Lausanne, BCH, 1015 Lausanne, Switzerland*
[b]*Department of Chemistry, University of California, Berkeley, CA 94720-1460, U.S.A.*
[c]*Département de Chimie, associé au CNRS, Ecole Normale Supérieure, 24 rue Lhomond, 75231 Paris cedex 05, France*

Received 6 March 2003; Accepted 10 March 2003

Key words: chemical shift anisotropy of imino protons, cross-correlation effects, hydrogen bonds, relaxation of double- and triple-quantum coherences, RNA kissing complexes

Abstract

The bond lengths and dynamics of intra- and intermolecular hydrogen bonds in an RNA kissing complex have been characterized by determining the NMR relaxation rates of various double- and triple-quantum coherences that involve an imino proton and two neighboring nitrogen-15 nuclei belonging to opposite bases. New experiments allow one to determine the chemical shift anisotropy of the imino protons. The bond lengths derived from dipolar relaxation and the lack of modulations of the nitrogen chemical shifts indicate that the intermolecular hydrogen bonds which hold the kissing complex together are very similar to the intramolecular hydrogen bonds in the double-stranded stem of the RNA.

Introduction

The measurement of cross-correlated relaxation rates in nuclear magnetic resonance (NMR) can provide remarkably detailed information about the structure and dynamics of biomolecules such as proteins and nucleic acids. Recent overviews of this rapidly-expanding field are now available (Daragan and Mayo, 1997; Anil Kumar et al., 2000; Schwalbe et al., 2001; Frueh, 2002). Some cross-correlation rates can be useful to supplement cross-relaxation rates (Overhauser effects) to provide information about internuclear distances (Riek, 2001; Chiarparin et al., 2001). Other cross-correlation rates provide valuable information about dihedral angles in proteins and nucleic acids and are therefore useful to complement Karplus-type studies of scalar couplings (Yang et al., 1997; Felli et al., 1999; Reif et al., 2000; Richter et al., 2000). To investigate the dynamics of biomolecules, some cross-correlation rates provide information that is complementary to the more common autocorrelated relaxation rates R_1(X), R_2(X) and steady-state NOE(X) (where X stands for heteronuclei ^{15}N or ^{13}C) (Lipari and Szabo, 1982; Peng and Wagner, 1994; Brutscher et al., 1997; Früh et al., 2001). These three rates depend on both CSA(X) and dipolar DD(X-H) autocorrelated relaxation, while cross-correlation allows one to focus on other combinations of relaxation mechanisms, for example CSA(X) and CSA(H) as treated in this work. Cross-correlation leads to the interconversion of specific coherences of the density operator while autocorrelated autorelaxation manifests itself merely through its dissipative character, i.e., through the decay of populations or coherences. Thus the conversion of, say, a density operator term $2I_xS_x$ into $2I_yS_y$ reflects a highly specific pathway, while the decay rate $R_2(S_x)$ of the single-quantum coherence S_x can be governed by a manifold of dissipative effects. If the 'initial' and 'final' coherences $2I_xS_x$ and $2I_yS_y$ are equivalent except for their phases, all parasitical 'leak-

*To whom correspondence should be addressed. E-mail: Geoffrey.Bodenhausen@ens.fr

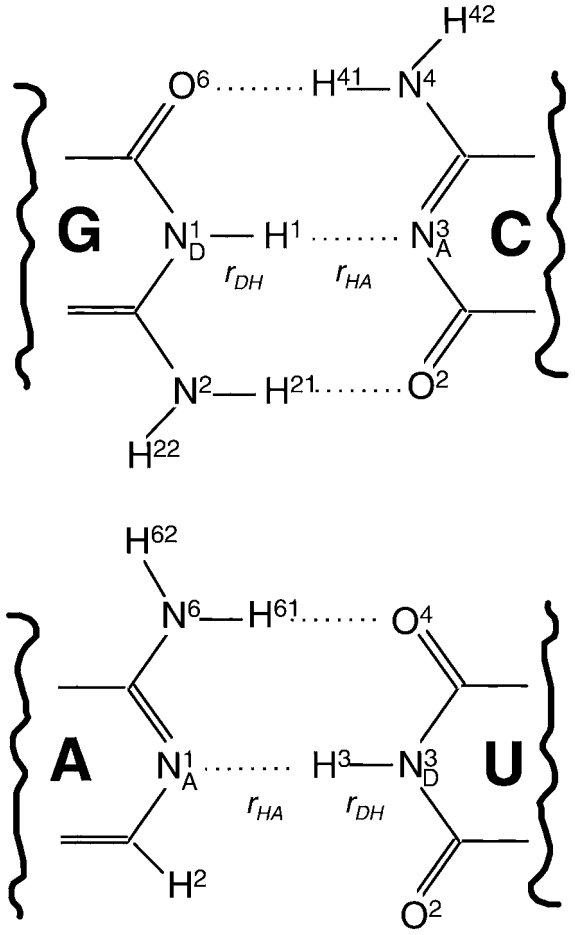

Figure 1. Hydrogen bonds in nucleic acid base pairs with conventional numbering (Markley et al., 1998). In this work, we focus on the N^1_D-$H^1 \cdots N^3_A$ bond of G–C pairs and on the N^3_D-$H^3 \cdots N^1_A$ bond of A–U pairs. In this work, the donor nitrogen atoms N^1_D of guanine and N^3_D of uracil are denoted D, and the components of their angular momentum D_x, D_y and D_z. The acceptor nitrogen atoms N^3_A of cytosine and N^1_A of adenine are denoted A, and their angular momentum components A_x, A_y and A_z.

age' pathways that contribute to their relaxation must be identical and therefore cannot affect the ratio of the expectation values $\langle 2I_yS_y\rangle/\langle 2I_xS_x\rangle$. In this work, we present a study of various cross-correlated relaxation effects in intra- and intermolecular hydrogen bonds in a biologically important RNA kissing complex.

Nucleic acids have been the subject of detailed relaxation studies, although perhaps less extensively than proteins. Figure 1 shows representations of the adenine-uracil (A-U) and guanine-cytosine (G-C) base-pairs with their conventional numbering (Markley et al., 1998). The imino hydrogen bonds can be denoted for simplicity by D-H$\cdots$A, with the 'donor' and 'acceptor' nitrogen atoms 'D' and 'A'. The cartesian components of angular momentum associated with the nuclei of these atoms will henceforth be denoted as D_x, D_y, D_z for the donor nitrogen, A_x, A_y and A_z for the acceptor nitrogen, and H_x, H_y, H_z for the imino proton. Auto- and cross-correlation rates due to the DD(^{15}N-^{1}H) and CSA(^{15}N) interactions have been determined in purine and pyrimidine bases (Akke et al., 1997; Boisbouvier et al., 1999; Hall and Tang, 1998; Riek, 2001; Pervushin, 2001; Dayie et al., 2002), and in the ribose or desoxyribose moieties of nucleic acids (Felli et al., 1999; Richter et al., 1999). Much interest has been focused on the hydrogen bonds which hold together Watson-Crick base pairs. It was discovered recently (Dingley and Grzesiek, 1998; Pervushin et al., 1998) that there is a non-vanishing $^{2h}J_{NN}$-coupling across the H-bond between the donor nitrogen D of guanine (or uracil) and the acceptor nitrogen A of cytosine (or adenine). In an earlier study (Chiarparin et al., 2001), this $^{2h}J_{NN}$-coupling was used to excite two-spin coherences involving both nitrogen nuclei D and A as well as three-spin coherences also involving the imino proton H. The relaxation rates of these coherences depend on the magnitudes and on the relative orientations of the tensors. Figure 2 shows the CSA tensors of the three nuclei D, H and A represented in the usual fashion by ellipsoids (Hu et al., 1998; Czernek, 2001). The principal axes of the dipolar tensors are of course aligned with the D-H and H-A bonds.

A kissing complex

This work is concerned with the structure and dynamics of a biologically important RNA kissing complex that comprises two identical hairpins containing a loop comprising four nucleotides (tetra-loop, 5′GACG3′, Figure 3). This 5′GACG3′ tetra-loop moiety has been shown to be critical in the dimerization and packaging processes of the genomic RNA of Moloney murine leukemia virus (De Tapia et al., 1998). This tetra-loop is highly conserved in the murine type C retrovirus. Recently, a high-resolution solution NMR study has been carried out on the RNA containing 18 nucleotides (H3-18, 5′-GGUGGGAGACGUCCCACC-3′) mimicking the native 5′GACG3′ tetra-loop combined with a stem region to investigate its structural and dynamic properties (Kim and Tinoco, 2000, Figure 3). This study led to the surprising discovery that two identical H3-18 molecules, the loop sequences of which are not self-complementary, form a kissing complex

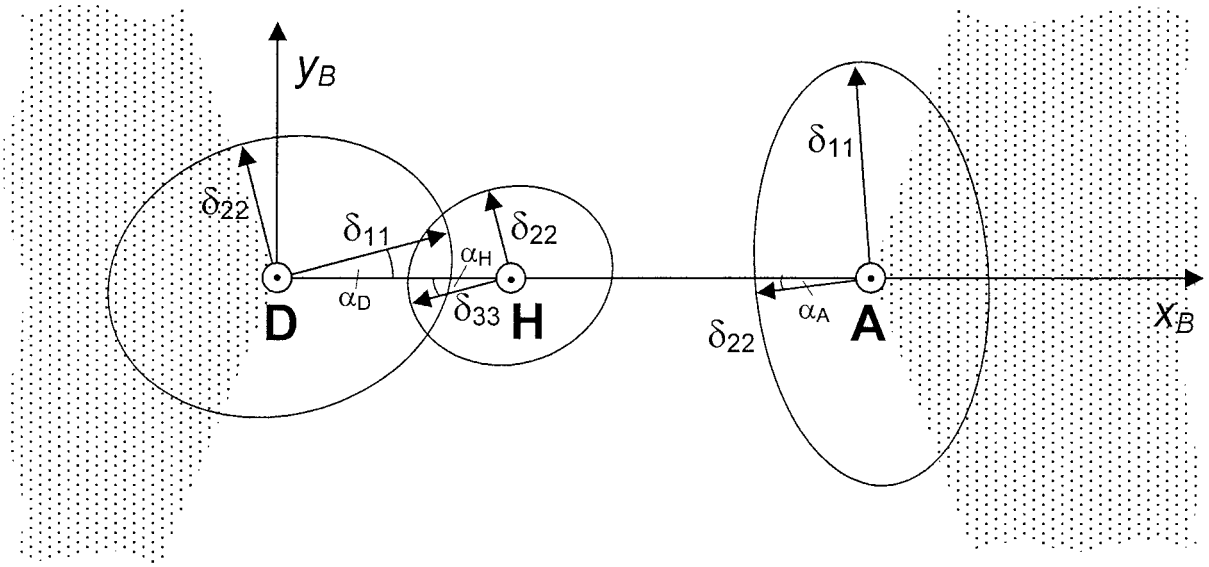

Figure 2. Orientations of the principal components δ_{ii} of the chemical shift anisotropy (CSA) tensors of the donor nitrogen D, the imino proton H and the acceptor nitrogen A under the simplifying assumption of collinearity. The coordinate system (x_B, y_B, z_B) is defined with respect to the base-pair, with the x_B axis parallel to the D-H-A axis, y_B in the plane of the base-pairs represented by dotted areas, and z_B perpendicular to this plane. Two of the principal components of each CSA tensor lie in the plane of the base-pairs spanned by the vectors x_B and y_B, the third one is parallel to z_B. The three components are usually ordered so that $\delta_{11} > \delta_{22} > \delta_{33}$. The angles α_D, α_H and α_A define the deviations of the principal components shown from the x_B axis.

linked through only two G-C base pairs in their tetra-loop regions. The formation of the kissing complex through intermolecular base-pairing between the two tetra-loops has been proposed to play an important role for the intermolecular recognition processes in the RNA dimerization and packaging processes of Moloney murine leukemia virus (Kim and Tinoco, 2000).

The structure of the dimer shown in Figure 3 has been determined by NMR (Kim and Tinoco Jr., 2000). The symmetry of the dimer ensures that the NMR responses of the two halves are superimposed. In particular, one can observe only 6 distinct imino resonances that belong to the stem, and only 1 imino resonance corresponding to the two intermolecular hydrogen bonds G11-C′10 and G′11-C10 (Figure 3). In contrast to an RNA fragment that we have investigated in an earlier study (Rüdisser and Tinoco Jr., 2000; Chiarparin et al., 2001), the stem of the molecule shown in Figure 3 only comprises properly matched Watson-Crick base-pairs.

In this work, we have used four distinct cross-correlation experiments, two of which have been specially developed to characterize the CSA's of imino protons. Three of the experiments use triple-quantum coherences with relaxation rates that are not affected by dipolar interactions between the active spins. This allows one to determine pure CSA/CSA relaxation rates which tend to be masked by dipolar relaxation in simpler experiments. In particular, the cross-correlation rate $R_{D,A}$ due to cross-correlation of the two nitrogen chemical shift anisotropies CSA(D) and CSA(A) can be extracted from suitable triple-quantum experiments (Chiarparin et al., 2001). In double-quantum experiments, one may observe the sum of the rate $R_{D,A}$ and of a contribution $R_{DH,HA}$ due to the interference of the two dipolar interactions DD(D-H) and DD(H-A). The difference between the triple- and double-quantum decay rates therefore yields the pure dipolar rate $R_{DH,HA}$, which primarily provides structural information on hydrogen bond lengths. We shall also present a new triple-quantum method designed to measure the cross-correlation rate $R_{D,H}$ due to interference between the donor nitrogen CSA(D) and the imino proton CSA(H), as well as the rate $R_{H,A}$ due to interference between CSA(H) and the acceptor nitrogen CSA(A). While the $R_{D,H}$ rate has been the subject of an earlier study (Pervushin, 2001), the $R_{H,A}$ rate has, to the best of our knowledge, never been investigated before. From these new experiments, we obtain what we believe to be the first experimental estimates of the principal values of the CSA tensors of imino

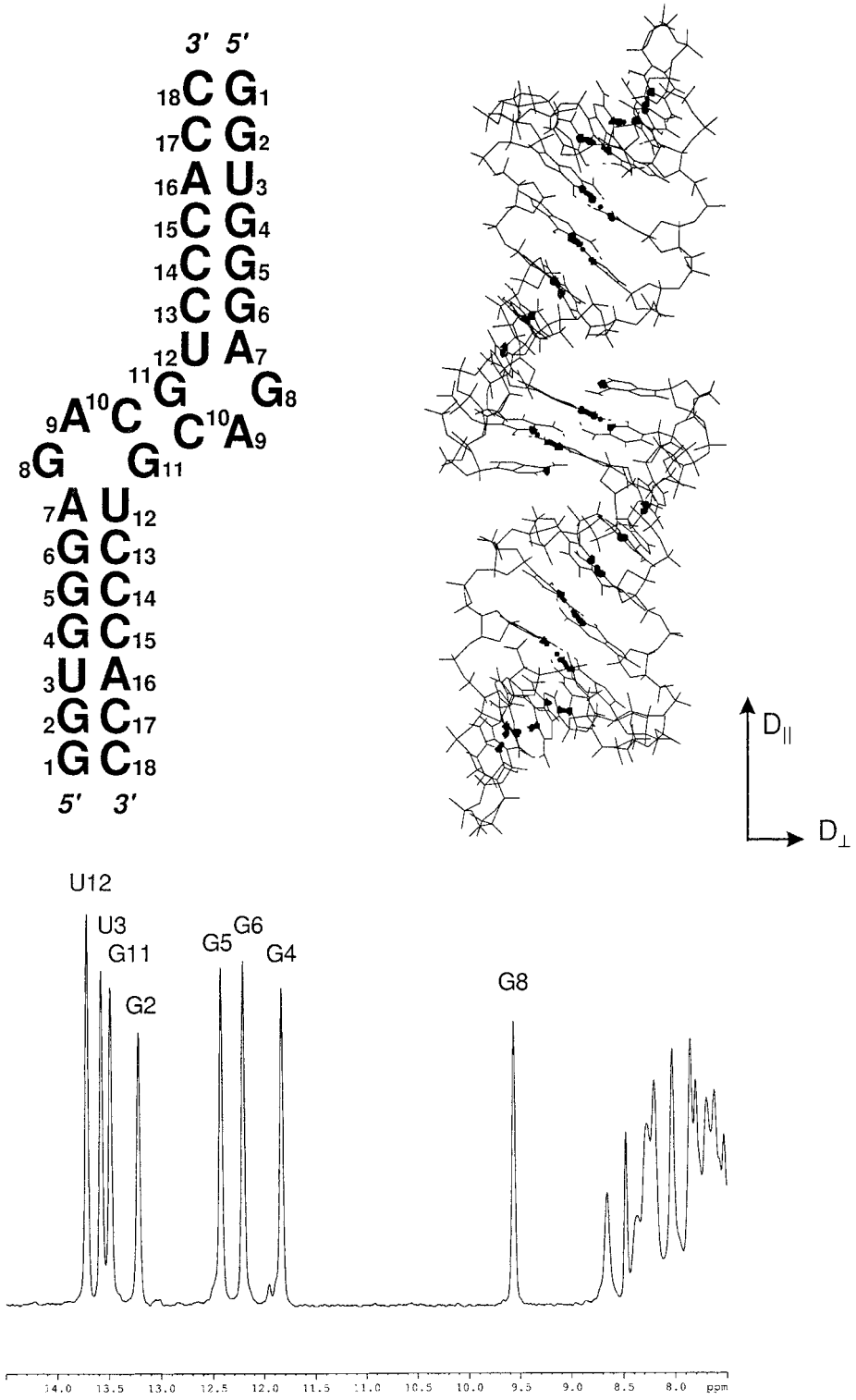

Figure 3. Top left: Schematic sketch of the H3-18 RNA with the sequence GGUGGGAGACGUCCCACC which forms a hairpin with a stem comprising 7 matched Watson–Crick base-pairs and a loop with 4 unpaired bases that can form 2 intermolecular base-pairs G11-C′10 and G′11-C10. The dimer is symmetrical, so that only 6 distinct imino protons in the stem and 1 imino proton in the kissing area can be observed. Top right: Structure of the kissing complex determined by NMR (Kim and Tinoco, 2000) with the principal axes of the anisotropic diffusion tensor D determined by nitrogen-15 relaxation (T_1, T_2 and NOE). Bottom: Proton spectrum of the imino region (128 scans at 400 MHz).

protons, which so far have only been the object of theoretical calculations (Czernek et al., 2000; Czernek, 2001)

Theory

The theory of cross-correlated relaxation has been discussed in detail elsewhere (Werbelow and Grant, 1977; Goldman, 1984; Anil Kumar et al., 2000; Chiarparin et al., 2001; Frueh, 2002) The DD/DD and CSA/CSA cross-correlation rates that are relevant to the D-H-A three-spin system in slow motion can be expressed in condensed form:

$$R_{DH,HA} = \left(\frac{\mu_0\hbar}{4\pi}\right)^2 \frac{\gamma_H^2\gamma_N^2}{r_{DH}^3 r_{HA}^3}\, J_{DH,HA}(0) \qquad (1)$$

$$R_{X,Y} = \tfrac{4}{9}\gamma_X\gamma_Y B_0^2 \sum_{\chi=1}^{3}\sum_{\xi=1}^{3} \sigma_{\chi\chi}^X \sigma_{\xi\xi}^Y J_{\chi\chi,\xi\xi}^{X,Y}(0), \quad (2)$$

where r_{DH} and r_{HA} are the internuclear distances, $\sigma_{\chi\chi}^X$ and $\sigma_{\xi\xi}^Y$ the principal components of the CSA tensors, and the other symbols have their usual meaning. The orientations of the base pairs with respect to the molecular frame can be taken from the PDB file 1F5U (Kim and Tinoco, 2000).

For the description of each cross-correlation effect a spectral density function must be defined:

$$J_{DH,HA}(\omega) = \tfrac{2}{5}\sum_{m=-2}^{2} \left\langle Y_2^m(\theta_{DH},\phi_{DH}) Y_2^{m*}(\theta_{HA},\phi_{HA})\right\rangle \times \frac{\tau_m}{1+\omega^2\tau_m^2}, \qquad (3a)$$

where θ_{DH}, ϕ_{DH} are the polar and azimuthal angles of the r_{DH} vector with respect to the diffusion tensor, while θ_{HA}, ϕ_{HA} are those of the r_{HA} vector.

$$J_{\chi\chi,\xi\xi}^{X,Y}(\omega) = \tfrac{2}{5}\sum_{m=-2}^{2} \left\langle Y_2^m(\theta_{\chi\chi},\phi_{\chi\chi}) Y_2^{m*}(\theta_{\xi\xi},\phi_{\xi\xi})\right\rangle \times \frac{\tau_m}{1+\omega^2\tau_m^2}, \qquad (3b)$$

where $\theta_{\chi\chi}$, $\phi_{\chi\chi}$ are the polar and azimuthal angles of the $\sigma_{\chi\chi}$ tensor component of nucleus X with respect to the diffusion tensor, and $\theta_{\xi\xi}$, $\phi_{\xi\xi}$ those of the $\sigma_{\xi\xi}$ component of nucleus Y.

The averaging represented by the angular brackets describes internal motions on the fast time scale, the effect of which can only be evaluated for a specific motional model. In this work we shall assume for the moment that the molecule is rigid; effects of local motions will be discussed below.

The correlation times for an axially symmetric diffusion tensor are defined as

$$\tau_m = 1/(6\,D_\perp - m^2(D_\perp - D_{||})). \qquad (4)$$

In our specific example, we have determined $D_{||}/D_\perp = 1.9$ and an average correlation time $\tau_c = (4D_\perp + 2D_{||})^{-1} = 8.7$ ns from autocorrelated relaxation of the donor nitrogen atoms, which yields $D_{||} = 2.8\cdot 10^7\ \mathrm{s}^{-1}$ and $D_\perp = 1.5\cdot 10^7\ \mathrm{s}^{-1}$, so that the three correlation times for $m = 0, \pm1, \pm2$ are equal to $\tau_m = 11.3$, 9.8, and 7.0 ns.

Experimental

All experiments A–D in Figure 4 are performed in the build-up fashion, consisting of (I) a reference experiment which measures the decay of the initial coherence as a function of the relaxation period T according to Equation 5, and (II) an experiment which measures the build-up of the coherence generated by interconversion (Equation 6). These experiments are also referred to as 'diagonal peak' (I) and 'cross peak' experiments (II), in analogy to NOESY experiments. Observing the build-up of a coherence is an alternative to measuring differential line broadening. As an example, the differential relaxation of the double- and zero-quantum parts of the coherence $4D_yH_zA_y$ in experiment A leads to a partial conversion into the term $4D_xH_zA_x$. The intensity of $4D_yH_zA_y$ is measured in (AI), that of $4D_xH_zA_x$ in (AII).

The signal intensities obey similar rules in all eight experiments A–D:

$$I_I = I_0\,\exp(-R_{ac}T)\,\cosh(R_{cc}T) \qquad (5)$$

$$I_{II} = I_0\,\exp(-R_{ac}T)\,\sinh(R_{cc}T), \qquad (6)$$

where R_{ac} and R_{cc} are the auto- and cross-corrrelated relaxation rates, respectively. The latter can be extracted from the ratio of the signal intensities of the two complementary experiments:

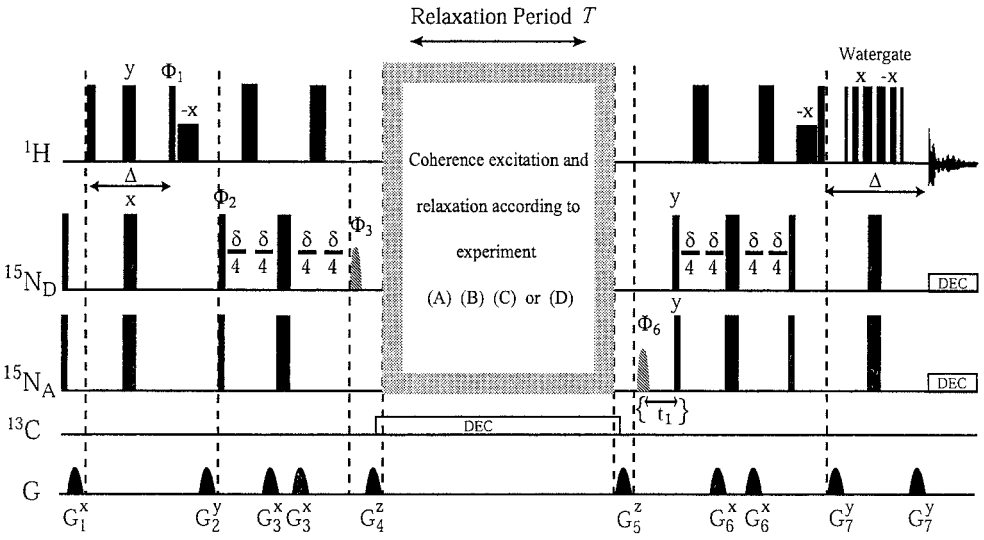
Relaxation Period T
Watergate
Coherence excitation and relaxation according to experiment (A) (B) (C) or (D)
DEC
DEC
DEC

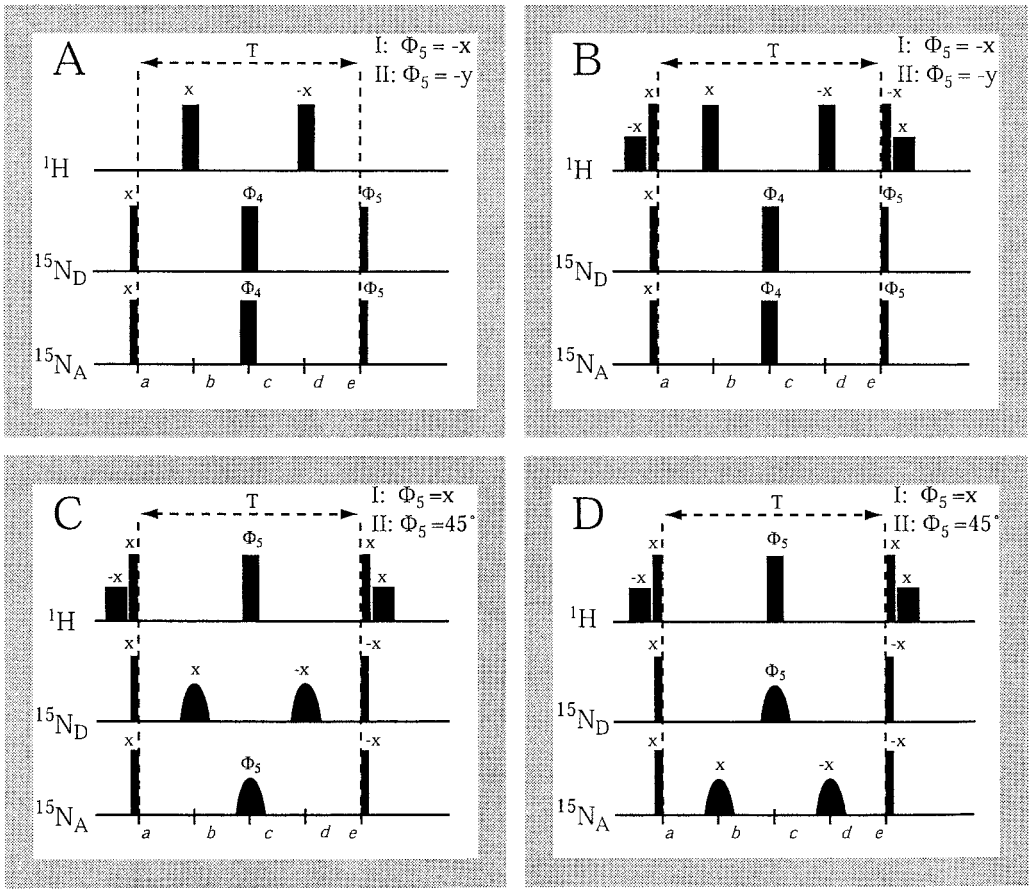
A
I: Φ5 = -x
II: Φ5 = -y
B
I: Φ5 = -x
II: Φ5 = -y
C
I: Φ5 =x
II: Φ5 =45°
D
I: Φ5 =x
II: Φ5 =45°

Figure 4. Pulse sequences used for the measurement of various cross-correlation rates in nucleic acids. Each of the four inserts can be modified either to detect the decay of the coherence that is initially excited ('diagonal peaks' obtained with experiments AI, BI, CI and DI) or to detect coherences that appear as a result of cross-correlated relaxation ('cross-peaks' observed with experiments AII, BII, CII, and DII). The experiments A use double- and zero-quantum coherences (DQC/ZQC) and allow one to measure $R_{D,A} + R_{DH,HA}$. Experiments B, C and D all use triple- and single-quantum coherences (TQC/SQC). Experiment B is designed to measure $R_{D,A}$, C to determine $R_{H,A}$, and D to measure $R_{D,H}$. Phase cycling: $\Phi_1 = (y, -y)_8$, $\Phi_2 = (x, x, -x, -x)_4$, $\Phi_3 = (-x)_4, (x)_4, (-x)_4, (x)_4$, $\Phi_6 = (y)_8, (-y)_8$, Φ_{rec} = x, −x, −x, x, −x, x, x, −x, −x, x, x, −x, x, −x, −x, x. In all experiments A, B, C and D, the π-pulses in the center of the relaxation interval T are cycled according to the EXORCYCLE prescription. In A and B, $\Phi_4 = (x)_{16}, (y)_{16}, (-x)_{16}, (-y)_{16}$, with $\Phi_5 = -x$ in AI and BI, and $\Phi_5 = -y$ in AII and BII. In CI and DI, $\Phi_5 = (x)_{16}, (y)_{16}, (-x)_{16}, (-y)_{16}$. In CII and DII, $\Phi_5 = (45°)_{16}, (135°)_{16}, (225°)_{16}, (315°)_{16}$. Unless specified otherwise, all other pulses are applied along the x axis. Delays: $\Delta = 4.5$ ms $\approx (2\,{}^{1}J_{DH})^{-1}$ since ${}^{1}J_{DH} \approx 88.5$ Hz, $\delta = 40$ ms (at 400 MHz) or $\delta = 30$ ms (at 600 MHz), which were optimized empirically since the conversion of $2D_yH_z$ into $4D_xH_zA_z$ via ${}^{2h}J_{DA} \approx 7$ Hz reaches a maximum before $\delta = (2\,{}^{2h}J_{DA})^{-1} = 71$ ms because of damping by auto-relaxation. The strengths of the gradients are expressed with respect to their maximum allowed amplitudes: $G_1^x = 19\%$, $G_2^y = 34\%$, $G_3^x = 23\%$, $G_4^z = 41\%$, $G_5^z = 51\%$, $G_6^x = 27\%$, $G_7^x = 45\%$. The carbon-13 nuclei were decoupled during the relaxation interval T by a GARP sequence; the nitrogen-15 nuclei were decoupled during proton acquisition by WALTZ-16. The selective π/2 pulse with phase Φ_3 was a time-reversed E-BURP-1 of 2.56 ms duration for a bandwidth (full width at half height) of 1.76 kHz (at 400 MHz) or 1.34 ms for 3.36 kHz (at 600 MHz) centered on the chemical shifts of the donor nuclei D (in experiments C and D at 146 ppm for guanine and at 161 ppm for uracil; in experiments A and B on the average shift at 153.5 ppm). The selective π/2 pulse with phase Φ_6 was an E-BURP-1 of 2.56 ms duration for a bandwidth of 1.76 kHz (at 400 MHz) and 1.22 ms for 3.69 kHz (at 600 MHz) centered on 195 ppm (cytosine), 220 ppm (adenine), or on the average at 208 ppm. Experiments C and D were performed twice, once for the A–U pairs and once for the G–C pairs, to avoid problems with the bandwidth of the selective pulses. In experiments A and B, which can be performed for both types of base-pairs at once, an average carrier frequency was chosen at 153.5 ppm.

$$R_{cc} = \frac{1}{T}\,\text{artanh}\frac{I_{II}}{I_I}. \tag{7}$$

If one uses short values T, so that the ratio of signal intensities (I_{II}/I_I) never exceeds 0.25, second-order effects can be neglected, and damping by the autorelaxation terms of Equations 5 and 6 is not too severe. The four different experiments illustrated in Figure 4 allow one to determine four different cross-correlation rates:

$$(A)\ R_{DH,HA} + R_{D,A} = (1/T)\ \text{artanh}\ (A_{II}/A_I) \tag{8}$$

$$(B)\ R_{D,A} = (1/T)\ \text{artanh}\ (B_{II}/B_I) \tag{9}$$

$$(C)\ R_{H,A} = (1/T)\ \text{artanh}\ (C_{II}/C_I) \tag{10}$$

$$(D)\ R_{D,H} = (1/T)\ \text{artanh}\ (D_{II}/D_I). \tag{11}$$

The dipolar rate $R_{DH,HA}$ can be obtained from the difference

$$R_{DH,HA} = (1/T)\ \text{artanh}\ (A_{II}/A_I) - (1/T)\ \text{artanh}\ (B_{II}/B_I). \tag{12}$$

The effects of various cross-correlated relaxation pathways on selected density operator terms during the relaxation period T are illustrated in Figure 5. Thus, if one initially excites the TQ/SQ coherence $D_yH_yA_y$, the rate $R_{D,A}$ leads to the conversion of it into $4D_xH_yA_x$, while $R_{H,A}$ generates a term $4D_yH_xA_x$, and the rate $R_{D,H}$ brings about a transformation of $4D_yH_yA_y$ into $4D_xH_xA_y$. If one initially excites a DQ/ZQ coherence $4D_yH_zA_y$, cross-correlations due to dipolar interactions also play a role: $R_{DH,HA}$ and $R_{D,A}$ both lead to a conversion of $4D_yH_zA_y$ into $4D_xH_zA_x$, $R_{DH,A}$ and $R_{D,HA}$ both lead to $2D_xA_x$, and $R_{D,DH}$ and $R_{HA,A}$ both generate $2D_yA_y$. These simple rules are only applicable to first order, i.e., if $R_{i,j}T \ll 1$ for all pairs of interactions *i,j*.

During the relaxation period T, the following effects occur: (i) Evolution under various chemical shifts; (ii) evolution under ${}^{1}J_{D,H}$ and ${}^{1h}J_{H,A}$ (these affect the DQ/ZQ coherences but not the TQ/SQ coherences); (iii) autocorrelated relaxation; (iv) cross-correlated relaxation. We have inserted various refocusing and/or inversion pulses in the T interval with the following aims: (i) Refocus the effects of chemical shifts and J-couplings, (ii) refocus the effects of all cross-correlations except the desired ones, and (iii) select the desired signals that one wishes to monitor, i.e., either 'diagonal peaks' in experiments AI, BI, CI and DI or 'cross-peaks' in experiments AII, BII, CII and DII.

The effects of the refocusing π-pulses inserted in the relaxation interval T are illustrated by the 'toggling frame' schemes of Figures 6A–D which are similar to those that were introduced for cross-correlation studies of proteins (Chiarparin et al., 1999). Consider for example Figure 6B which describes experiments BI and BII, both of which start with the TQ/SQ coherence $4D_yH_yA_y$. The evolution under the chemical shifts Ω_N and Ω_H and the effects of the cross-correlation rates

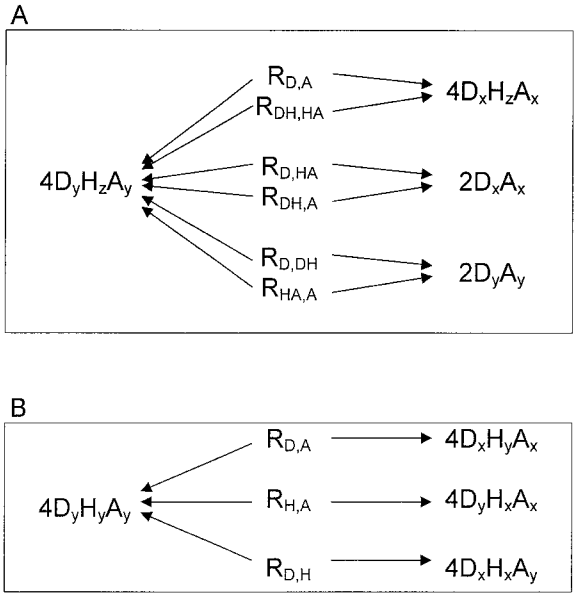

Figure 5. Cross-correlation pathways (A) starting from the DQ/ZQ coherence $4D_yH_zA_y$ and (B) from the TQ/SQ coherence $4D_yH_yA_y$. A symbol such as $R_{D,HA}$ represents the cross-correlation rate involving the CSA of the donor D and dipole-dipole interaction HA between the imino proton H and the acceptor nitrogen A. In (A), cross-correlations such as $R_{D,DA}$ and $R_{DA,A}$ have been neglected because the nitrogen-nitrogen dipole-dipole interaction DA is quite small. In (A), the cross-correlations involving the CSA of the imino proton H do not effect the outcome because they commute with the operator $4D_yH_zA_y$ representing the DQ/ZQ coherence. The TQ/SQ coherence $4D_yH_yA_y$ in (B) does not experience any cross correlation with any dipolar interaction because the relevant operators commute with this density operator term. The pulse schemes during the relaxation period are designed so that the effects of all cross correlations except for the desired ones are cancelled (see Figure 6).

$R_{D,H}$ and $R_{H,A}$ are all cancelled (since they change their signs), while only the effect of $R_{D,A}$ is preserved. As a result, all terms into which $4D_yH_yA_y$ could be converted are suppressed, except for $4D_xH_yA_x$. The separation of the cross-correlation rates $R_{H,A}$ and $R_{D,H}$ is technically more demanding, since the donor and acceptor nitrogens have to be differentiated by applying selective pulses as shown in Figure 6C and 6D.

Switching between 'diagonal peak' and 'cross peak' experiments I and II can be achieved as follows. In experiment AI, the phase of the last pulse in the T interval is set to $\Phi_5 = -x$ to convert $4D_yH_zA_y$ into $4D_zH_zA_z$, while $4D_xH_zA_x$ remains invariant and cannot be transformed into any observable signal. In experiment AII the phase is $\Phi_5 = -y$, which converts $4D_xH_zA_x$ to $4D_zH_zA_z$, while the coherence $4D_yH_zA_y$ will be filtered out. The same principle is used in experiments BI and BII. In experiments CI and CII however, the selection is achieved in a novel manner. As we shall see below, the cross-correlated relaxation rate $R_{H,A}$ converts $4D_yH_yA_y$ into $4D_yH_xA_x$, which cannot be reconverted into $4D_zH_zA_z$ by means of a single nitrogen pulse. However, by shifting the phase Φ_5 of the refocusing pulses applied to the acceptor nitrogens and to the protons by 45°, one can change the phase of the coherence at the time of the echo by converting A_x into A_y and H_x into H_y. By converting $4D_yH_xA_x$ into $4D_yH_yA_y$, one can effectively 'unwind' the effect of the cross-correlated relaxation rate $R_{H,A}$. Thus in experiment CI the phases of the refocusing pulses applied to the acceptor nitrogens and to the protons are both $\Phi_5 = 0°$ (i.e., both along the x-axes of their respective rotating frames), so that the initial coherence $4D_yH_yA_y$ will be detected. In experiment CII we set both of these phases to $\Phi_5 = 45°$, so that one observes again the $4D_yH_yA_y$ term although it now arises from a combination of cross-correlated relaxation $R_{H,A}$ and the phase-shifts of the π-pulses.

For the sake of illustration, the conversion of the density operator term $4D_yH_yA_y$ under the combined effects of $R_{H,A}$ and of the phase-shifted selective refocusing pulses will be given in detail for experiment CII.

$$
\begin{aligned}
(II)\ 4D_yH_yA_y &\xrightarrow{\frac{1}{2}R_{H,A}T} 4D_yH_yA_y\cosh(\tfrac{1}{2}R_{H,A}T) \\
&\quad + 4D_yH_xA_x\sinh(\tfrac{1}{2}R_{H,A}T) \\
&\xrightarrow{\pi^A(\phi_5=45°)}\xrightarrow{\pi^H(\phi_5=45°)} 4D_yH_xA_x\cosh(\tfrac{1}{2}R_{H,A}T) \\
&\quad +4D_yH_yA_y\sinh(\tfrac{1}{2}R_{H,A}T) \\
&\xrightarrow{\frac{1}{2}R_{H,A}T} 4D_yH_xA_x\cosh(\tfrac{1}{2}R_{H,A}T)\cosh(\tfrac{1}{2}R_{H,A}T) \\
&\quad +4D_yH_yA_y\cosh(\tfrac{1}{2}R_{H,A}T)\sinh(\tfrac{1}{2}R_{H,A}T) \\
&\quad +4D_yH_yA_y\sinh(\tfrac{1}{2}R_{H,A}T)\cosh(\tfrac{1}{2}R_{H,A}T) \\
&\quad +4D_yH_xA_x\sinh(\tfrac{1}{2}R_{H,A}T)\sinh(\tfrac{1}{2}R_{H,A}T) \\
&= 4D_yH_xA_x\cosh(R_{H,A}T) \\
&\quad +4D_yH_yA_y\sinh(R_{H,A}T). \qquad (13)
\end{aligned}
$$

Note that the resulting $4D_yH_yA_y$ term is proportional to $\sinh(R_{H,A}T)$, which corresponds to the desired cross-correlation pathway. On the other hand, the reference experiment CI uses phases $\pi^A(\Phi_5 = 0°)$ and

$\pi^{H}(\Phi_5 = 0°)$ in the middle of the T interval:

$$(I)\ 4D_yH_yA_y \xrightarrow{\frac{1}{2}R_{H,A}T} \xrightarrow{\pi^{A}(\phi_5=0°)} \xrightarrow{\pi^{H}(\phi_5=0°)} \xrightarrow{\frac{1}{2}R_{H,A}T} 4D_yH_yA_y\cosh(R_{H,A}T) + 4D_yH_xA_x\sinh(R_{H,A}T). \quad (14)$$

We shall again select the term $4D_yH_yA_y$, but this time it is proportional to $\cosh(R_{H,A}T)$.

Experiment D has been designed to measure $R_{D,H}$ and is analogous to C, except that the selective pulses on donor and acceptor nitrogens have been interchanged.

As may be appreciated in Figure 4, all four experiments A, B, C, and D discussed in this work use the same sequence to prepare a state of longitudinal three-spin order $4D_zH_zA_z$ just before the relaxation period T, in analogy to the earlier work of Chiarparin et al. (2001). The experiments start with an INEPT sequence to generate antiphase coherence $2D_xH_z$ of the donor nitrogen. Then, the ${}^{2h}J_{D,A} = 6$–7 Hz coupling across the hydrogen bond is allowed to act during the δ interval to generate a coherence $4D_yH_zA_z$. Note that ${}^{1h}J_{H,A} = 2.0$–3.6 Hz is much smaller than ${}^{2h}J_{D,A} = 6$–7 Hz (Pervushin et al., 1998; Dingley and Grzesiek, 1998). A selective $\pi/2$ pulse with phase $\Phi_3 = +x$ or $-$x on the donor nitrogen D then converts $4D_yH_zA_z$ into longitudinal three-spin order $\pm 4D_zH_zA_z$. The $\pi/2$ pulse with phase Φ_2 has to act only on the donor D and could thus be replaced by a selective pulse which is symmetrical but time-reversed with respect to Φ_3. Unwanted coherences which might arise from pulse imperfections are eliminated by means of a pulsed field gradient G_4.

The $4D_zH_zA_z$ term can be easily converted into two- or three-spin coherences. In experiment A, DQ/ZQ coherence $4D_yH_zA_y$ is generated by applying a $\pi/2$ pulse on both nitrogens D and A, while an additional $\pi/2$ proton pulse generates TQ/SQ coherence $4D_yH_yA_y$ in experiments B, C, and D. The four experiments differ in the way that the multiple quantum coherences are manipulated during the relaxation period T as discussed above.

After the relaxation interval T, the operator terms of interest are converted back into $4D_zH_zA_z$. Remaining undesirable coherences (except for homonuclear zero-quantum coherences) are dephased by the pulsed field gradient G_5. In conjunction with later pulse imperfections, remaining zero-quantum coherences of this type may affect experiments of type II in particular, where one must focus on weak signals. Zero-quantum leakage signals tend to be proportional to the signal intensities in experiments of type I and may therefore lead to a small offset if one plots the build-up of the ratio of signal intentities II/I.

The subsequent coherence transfer steps are essentially symmetrical with respect to the beginning of the sequence. It is possible to insert an evolution time t_1 to label the coherence by the chemical shift of the acceptor. This would lead to a 2D-spectrum that could help to resolve peaks if the imino protons overlap. The suppression of the intense water signal is performed by a combination of flip-back pulses (Grzesiek and Bax, 1993) and a 3-9-19 WATERGATE (Piotto et al., 1992). The pulsed field gradients used in the sequence of Figure 4 were designed for probes with three orthogonal gradients, but they can readily be adapted for probes that have only z-gradients (Chiarparin et al., 2001).

Selective refocusing pulses

Separate experiments were carried out for G–C and A–U pairs. During the relaxation interval T, the nitrogen-15 carrier frequency was set to 172.0 ppm for G–C pairs, in the center between the donor and acceptor regions which are $\pm$ 24.8 ppm ($\pm$ 1.5 kHz in a 600 MHz spectrometer) apart. For A–U pairs, these frequencies are 191.7 ppm $\pm$ 29.6 ppm ($\pm$ 1.8 kHz). Phase-modulation was used to shift the effective carrier frequency to the donor or acceptor region. If G–C and A–U experiments are recorded separately, the regions to be covered are reduced to about 140 Hz.

The demands on selectivity are not easy to fulfill, since the pulses should have no appreciable effect off-resonance, i.e., a π^{A} pulse ideally should have no effect on D_x and D_y coherences. Vice-versa, a π^{D} pulse should have no effect on A_x and A_y terms. In particular, Bloch–Siegert phase-shifts (Emsley and Bodenhausen, 1990) are undesirable. As can be derived from Equation 13, these cannot generate anomalies in the observable terms, as long as the hard proton refocusing pulse in the center of the T interval works properly, but they can lead to a drastic signal attenuation. A RE-BURP ('refocusing band-selective pulse with uniform response and pure phase') (Geen and Freeman, 1991) with a bandwidth $\Delta\nu = 2.4$ kHz (for which a pulse duration $\tau_p = 2.423$ ms is required) appears attractive, since the z-component is attenuated less than 5% off-resonance, outside the so-called transition region. But the phases of D_x and D_y coherences are strongly affected by a RE-BURP pulse applied to the acceptor A even 3 kHz off-resonance.

For this reason, we have chosen an r-SNOB ('selective excitation for biochemical applications') pulse (Kupce et al., 1995), which gives a relatively narrow excitation region ($\Delta\nu = 962$ Hz) for the same pulse length $\tau_p = 2.423$ ms. The pulses were calibrated and their effects were verified by simulations and experiments. To avoid artifacts due to pulse imperfections it is preferable to measure $R_{H,A}$ and $R_{D,H}$ from build-up curves rather than from the difference of single- and triple-quantum intensities in constant-time 2D spectra. In this way, Bloch-Siegert shifts cause the same signal attenuation in both experiments I and II.

In experiments C and D, the total duration of the three selective nitrogen pulses ($3\tau_p = 7.3$ ms) is comparable to the relaxation period T. The latter should not be too long to avoid second-order effects and excessive damping by autorelaxation. Thus relaxation during the pulses must be taken into consideration. We consider the trajectory of the magnetization of a spin that is refocused by an r-SNOB pulse, which leads to a slightly reduced effective relaxation period T_{eff}:

$$T_{eff} = T - 3\tau_p \cdot \left(1 - \frac{1}{\tau_p} \int_0^{\tau_p} \left| \frac{I_{tr}(t)}{I_{tr,0}} \right| \, dt \right), \tag{15}$$

where T is the overall relaxation period, τ_p the length of each of the 3 selective pulses and $I_{tr}(t)$ is the time-dependent transverse component of the magnetization of the donor or acceptor nucleus during the pulse. The reduction factor in brackets is only 0.10, since the magnetisation lies in the transverse plane for most of the duration of the pulse. A more rigorous treatment is given by Griesinger and Ernst (1988).

Data acquisition and processing

Experiments A and B were performed on Bruker Avance 400 and 600 MHz spectrometers, while experiments C and D were only carried out at 600 MHz. The temperature was 296 K for all experiments. To monitor the decay and build-up of the signals, the peak intensities were measured for experiments A and B at $T = 0.4$, 8, 12, 16, 24 ms (400 MHz) and $T = 0.4$, 12, 16, 20, 24 ms (600 MHz), for C at $T = 12$, 16, 20, 24, 28 ms (600 MHz), and for D at $T = 12$, 17.2, 22.4, 28 ms (600 MHz). While experiments C and D were performed separately for A–U and G–C base pairs, experiments A and B, which do not require any selective pulses in the relaxation period T, could be carried out for A–U *and* G–C base pairs at once.

For experiment AI, 2 K scans were accumulated at 400 MHz, and 3 K at 600 MHz. For experiment AII, 8 K scans were recorded at 400 MHz and (depending on the duration of T) 15–16 K at 600 MHz. For experiment BI, the scan numbers were 2 K at 400 MHz and 2–4 K at 600 MHz, while experiment BII required 20 K scans at 400 MHz and 18 K at 600 MHz. For experiments CI, CII, DI and DII, we accumulated 3–5 K, 18–24 K, 4 K, and 27–28 K scans, respectively.

The spectra were processed by XWIN-NMR, the peak intensities being determined by Gaussian deconvolution. The fitting of the intensity ratios of Equations 8–11 to hyperbolic tangens functions was performed by means of the Marquardt–Levenberg algorithm (see Press et al., 1986), and the errors determined from the covariance matrix.

Results and discussion

Experiments A and B

The rates $R_{D,A}+R_{DH,HA}$ and $R_{D,A}$ were obtained from the double- and triple-quantum experiments A and B at two different static fields corresponding to 400 and 600 MHz, as shown in Figure 7. The lower part of this figure shows the dipolar rates $R_{DH,HA}$ obtained from the difference of the rates plotted in the upper part. The most striking feature is the difference between G–C and A–U pairs for $R_{D,A} + R_{DH,HA}$ and for $R_{D,A}$, but not for the difference $R_{DH,HA}$. There are also small variations among the $R_{D,A}$ rates of the five G–C base pairs, both at 400 and 600 MHz. The rates are of course enhanced in the latter case by a factor $(600/400)^2 = 2.25$, as expected. In particular, the intermolecular base pair G11-C′10, which is specific to the kissing complex under investigation, shows rates $R_{D,A}$ that are somewhat higher than the average values of the other G–C base pairs in both experiments A and B at both fields. G2-C17 however shows a relatively low value.

Calculations of cross-correlation rates due to anisotropic chemical shifts

We have used Equations 1–4 to predict various rates, using parameters known from independent studies wherever possible. Geometrical properties, in particular the orientations of the base pairs in the molecule, can be derived from the NMR structure of the PDB file 1F5U (Kim and Tinoco, 2000). We make the simplifying assumptions that the donor nitrogen D, the imino

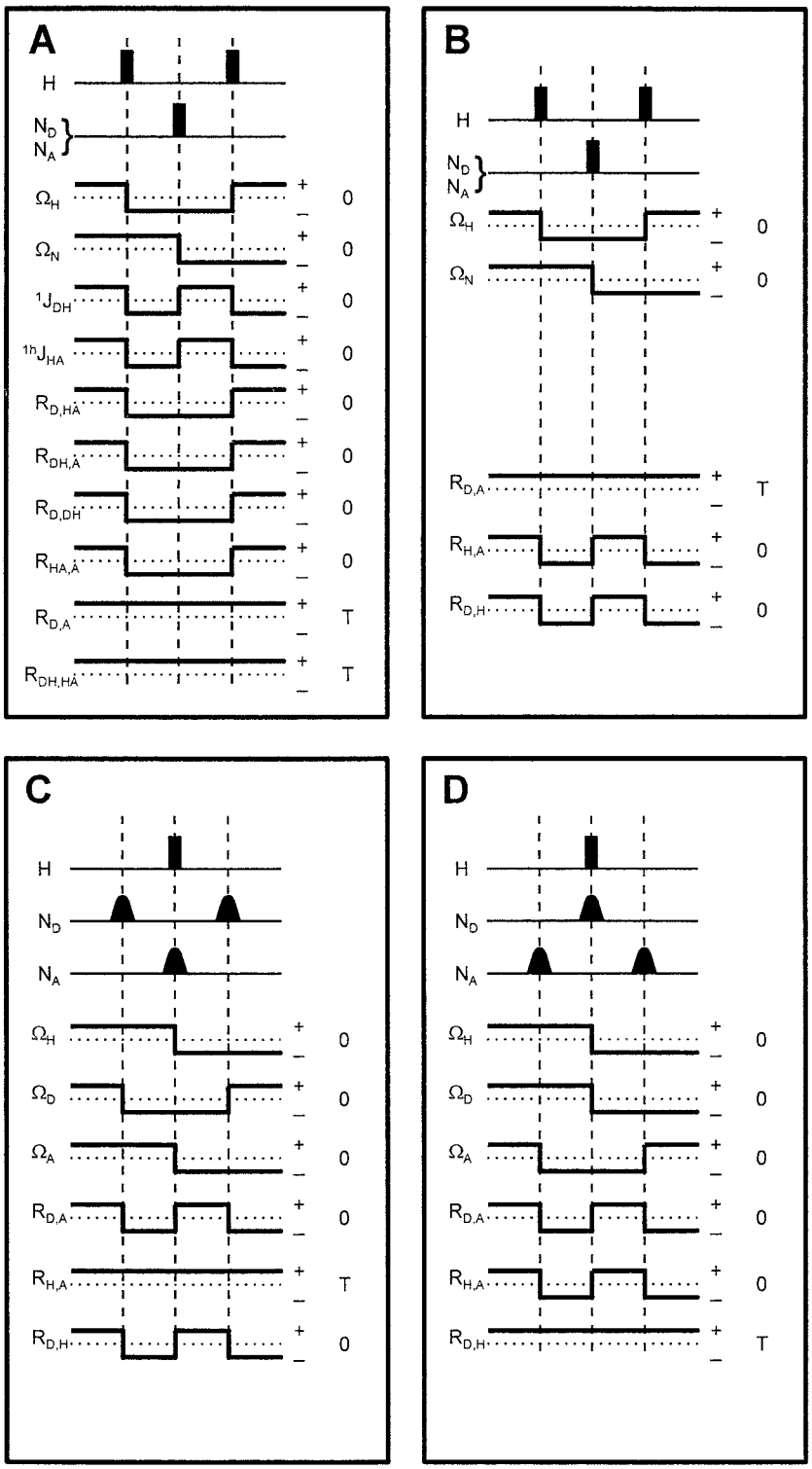

Figure 6. Toggling schemes (Chiarparin et al., 1999) where a sign alternation denotes a change of the effective sign of Ω, J or R in the course of the relaxation interval T, corresponding to experiments A, B, C and D of Figure 4. The diagrams demonstrate how the chemical shifts Ω_H and Ω_N and the J-couplings are refocused, and how cross-correlation effects listed in Figure 5 – except for the desired ones – are cancelled to first order. A zero on the right-hand side indicates that the relevant interaction has been cancelled, a symbol T means that the interaction is effective over the entire relaxation interval. (A) Effects of various interactions on $D_yH_zA_y$ in experiment A which allows one to determine $R_{D,A} + R_{DH,HA}$. (B) Effects of various interactions on $D_yH_yA_y$ in experiment B to measure $R_{D,A}$. (C) Effects in C designed to determine $R_{H,A}$. (D) Effects in D to measure $R_{D,H}$. In the TQ/SQ coherence in experiments B–D, the J-couplings have no effect.

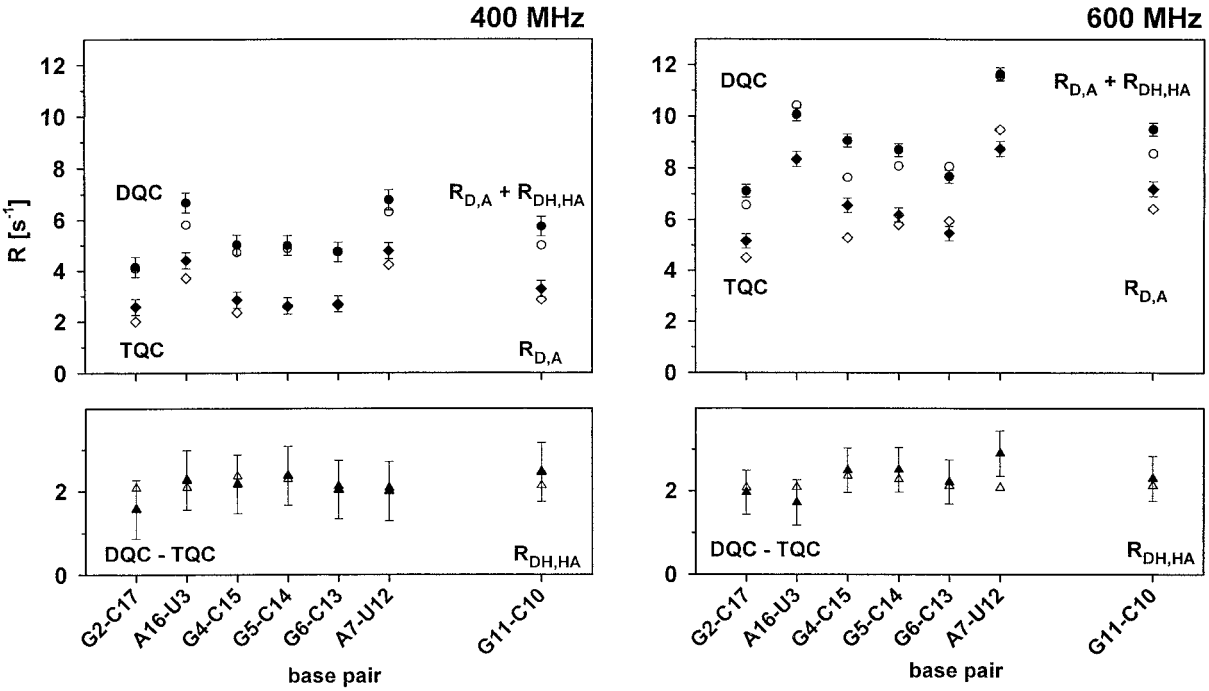

Figure 7. Experimental cross-correlation rates in the RNA of Figure 3 recorded at 296 K and at 400 MHz (left) and at 600 MHz (right): (circles) Combined effects $R_{D,A} + R_{DH,HA}$ from experiment A, (lozenges) pure CSA/CSA relaxation $R_{D,A}$ from experiment B, and (triangles) pure dipolar contribution $R_{DH,HA}$ obtained from the difference of these two rates. Open symbols represent calculated values (see text).

proton H and the acceptor nitrogen A are collinear and that the two bases of each pair lie in the same plane. The CSA tensors of both donor and acceptor nitrogens have been measured experimentally for isolated nucleic acids by solid-state nitrogen-15 MAS NMR by Anderson-Altmann et al. (1995) and Hu et al. (1998), backed up by DFT calculations to determine the orientations of the principal axes with respect to the molecular framework. Extensive ab-initio calculations by Czernek (2001) for the donor nitrogen CSA are consistent with the measurements of Hu et al. (1998), and provide more insight into the effects of hydrogen bonds. We have used Hu's calculated tensors for the acceptors and Czernek's tensors for the donors. Czernek also calculated CSA tensors for the imino protons. To the best of our knowledge, our work represents the first attempt to determine imino proton CSA tensors experimentally. The anisotropy of the CSA tensors requires a full tensor treatment according to Equations 2–4. If one made the crude assumption that the CSA tensors are axially symmetric, this would lead to rates that greatly diverge from our experimental observations.

With the parameters in Table 1, the measured rates $R_{D,A}$ can be reasonably well predicted with Equations 2–4. The intrinsic differences in the CSA tensors of the acceptor nitrogens of adenine and cytosine explain the differences in the $R_{D,A}$ rates of G–C and A–U base pairs. The calculations show that there are small variations in the $R_{D,A}$ for the same types of base pairs due to the orientations of the base pairs with respect to the diffusion tensor (Figure 7). The agreement with the observed variations is not perfect. They are in the range of the experimental precision and the accuracy of the model. However, they can – at least partially – explain the relatively low rate $R_{D,A}$ of G2–C17 and the relatively high rate of G11-C′10.

Thus there is no evidence that the intermolecular G-C base pair features significantly different CSA tensors or significantly greater internal mobility, nor a greater propensity to base-pair opening, than in the stem. This is consistent with evidence from the dipolar $R_{DH,HA}$ rate.

Internal motions on the μs-ms timescale can lead to significant CSM/CSM contributions to the cross-correlation rate $R_{D,A}$ if these motions lead to concerted changes of the chemical shifts of both nitrogens, as assumed by Chiarparin et al. (2001) for an RNA hairpin with base-pair mismatches. In our kissing dimer however, where all base-pairs are properly matched, the

Table 1. Principal components δ_{ii} of the CSA tensors of the donor nitrogen nuclei calculated by Hu et al. (1998) and the acceptor nitrogen nuclei calculated by Czernek (2001), supported by experimental observations, converted into the chemical shift scale used in this work. In brackets the difference with respect to the isotropic average $\Delta\delta_{ii} = \delta_{ii} - \delta_{iso}$. The meaning of the angles α_D and α_H for donors and acceptors is shown in Figure 2

	G–C		A–U	
	G (Donor)	C (Acceptor)	U (Donor)	A (Acceptor)
δ_{11} [ppm]	240 (+80)	311 (+121)	248 (+64)	373 (+153)
δ_{22} [ppm]	153 (−6)	224 (+34)	198 (+14)	296 (+76)
δ_{33} [ppm]	85 (−74)	34 (−156)	108 (−76)	−9 (−229)
δ_{iso} [ppm]	159	190	184	220
α_D, α_H [deg]	18	0	19	0

agreement between the experiments and calculations based on CSA/CSA cross-correlation alone is good, implying that the contributions due to CSM/CSM must be negligible.

Dipole/dipole cross correlation rates

The CSA/CSA cross-correlation rates $R_{D,A}$ shown in Figure 7, determined by the triple-quantum experiment B, show similar patterns as the rates of experiment A. As a result, the subtraction of the rates $R_{D,A}$ of experiment B from the rates $R_{DH,HA} + R_{D,A}$ of experiment A yields fairly constant values for the dipolar cross-correlation rates $R_{DH,HA}$. It is satisfactory to notice that the dipolar rates are largely field-independent, as they are supposed to be. The variations in the $R_{DH,HA}$ rates measured at 400 MHz, which closely agree with our calculations, are again due to the orientations of the tensors of the dipolar couplings (the unique axes of which lie along the r_{DH} and r_{HA} vectors) with respect to the anisotropic diffusion tensor. Only for A7-U12 do the rates $R_{DH,HA}$ differ between the experiments at 400 and 600 MHz, which seems to be mostly the result of subtraction errors that appear to be exacerbated by the large $R_{D,A}$ rates. Such errors may become a problem at higher fields, where the $R_{D,A}$ rates tend to dominate.

It is straightforward to estimate the hydrogen bond length r_{HA} from the rates $R_{DH,HA}$, according to Equations 1 and 3a. Assuming r_{DH} =1.01 Å we obtain a best fit with $r_{HA} = 2.05$ Å for all base-pairs. This value lies near the upper limit of the expected range 1.75–2.05 Å. Since the motions of the two vectors $\vec{r}_{D,H}$ and $\vec{r}_{H,A}$ are to a large extent correlated, one has to account for the attenuating effect of internal motions on the rate $R_{DH,HA}$. This is described by Riek (2001), who finds by means of other cross-correlation rates an apparent hydrogen bond length $r_{HA}^{app} = \left(1/S^2\right)^{1/3} r_{HA}$ which is increased by internal motions. The factor S^2 is however ill-defined for anisotropic tumbling as in our case (S. Ravindranathan, personal communication). Nevertheless it is evident that we qualitatively observe a similar effect as described by Riek, i.e., an increase of the apparent bond length due to internal motions. Note that fast internal motions do not necessarily attenuate the $R_{D,A}$ rate.

Apart from the above discussion about the absolute value of r_{HA}, we will briefly compare the variations of the rates $R_{DH,HA}$ between different residues. Taking into consideration an error in the rates of ± 0.5 s^{-1} there is an uncertainty in r_{HA} of about 0.15 Å. Due to errors stemming from subtraction of $R_{D,A}$ from $R_{D,A}+R_{DH,HA}$, our method is probably not the best for the accurate determination of hydrogen bond lengths. Apart from the inaccuracy of the $R_{DH,HA}$ rate of the A7-U12 pair, there is no significant evidence for any intrinsic variations in hydrogen bond lengths within the above precision. This stands in contrast to our earlier work (Chiarparin et al., 2001) on an RNA fragment with mismatched base-pairs, where the dipolar cross-correlation rates $R_{DH,HA}$ were found to be lower for hydrogen bonds in the vicinity of mismatched pairs. In the kissing complex, there are no mismatches in the stem, and the fact that the dipolar rates $R_{DH,HA}$ are the same for both A–U and G–C base pairs implies that there are no significant differences in the hydrogen bond lengths. It is remarkable that even the *inter*molecular hydrogen bond between G11 and C10 appears to have the normal 'canonical' bond length.

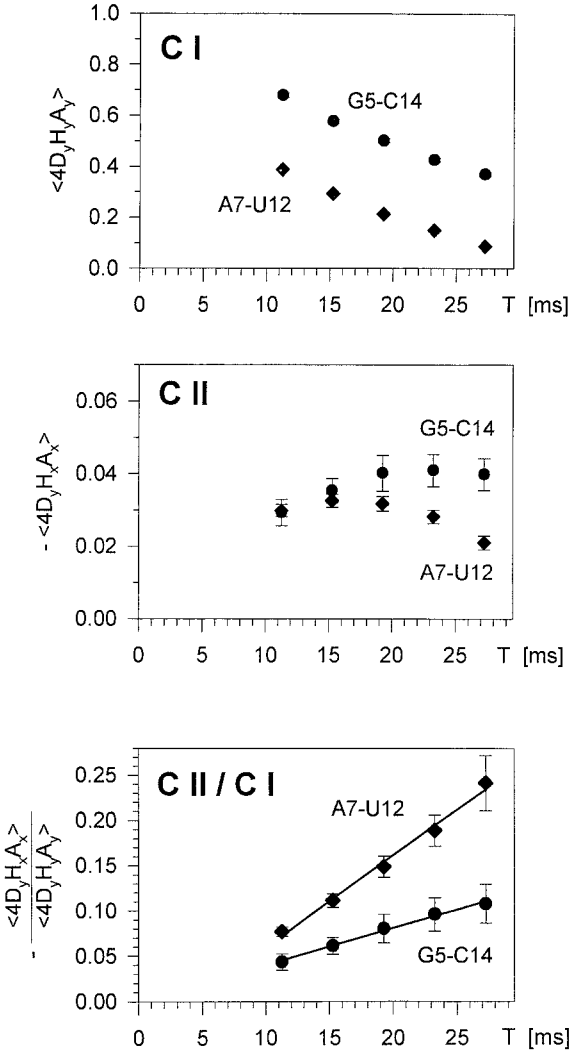

Figure 8. Decay and build-up curves recorded with experiments CI and CII at 600 MHz and 296 K to determine $R_{H,A}$ of A7-U12 (lozenges) and G5-C14 (circles). Top: Decay of $\langle D_y H_y A_y \rangle$ due to auto- and cross-correlated relaxation. Center: Build-up of $-\langle D_y H_x A_x \rangle$ due to cross-correlated relaxation, damped by autorelaxation. Bottom: Ratio of the intensities of $-\langle 4D_y H_x A_x \rangle / \langle 4D_y H_y A_y \rangle$.

Experiments C and D: Chemical shift anisotropy of imino protons

Figure 8 shows the decay and build-up of signal intensities in experiment C recorded at 600 MHz. Figure 9 shows the experimental rates $R_{H,A}$ (filled circles) from experiment C, and the rates $R_{D,H}$ (filled lozenges) from experiment D. There are significant correlations between each of the two rates $R_{H,A}$ and $R_{D,H}$ and the rate $R_{D,A}$. The $R_{H,A}$ rates are generally higher than

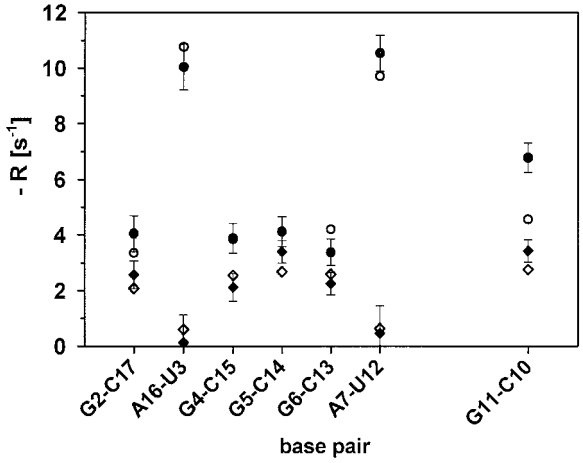

Figure 9. Rates $R_{D,H}$ (lozenges) and $R_{H,A}$ (circles) due to correlated fluctuations of the chemical shifts of the imino proton H and of either donor D or acceptor nitrogen A, recorded at 600 MHz. Calculated rates (open symbols) were fitted to experimental rates (filled symbols) by adjusting the principal components of the imino proton CSA tensor.

$R_{D,H}$, which is not surprising since the anisotropies of the acceptor nitrogens are more pronounced than the CSA's of the donors (see Table 1). Similar arguments allow one to explain the fact that $R_{H,A}$, like $R_{D,A}$, is higher for A–U pairs than for G–C pairs, because the CSA's of the acceptor nitrogens are significantly greater in adenine than in cytosine.

The fact that the rates $R_{D,H}$ are much lower in A–U pairs than in G–C pairs is however surprising. In principle, this could be due to differences between the CSA's of the donor nitrogen nuclei U and G, but such variations would be in contradiction not only with our $R_{D,A}$ rates, but also with calculations (Hu et al., 1998; Czernek, 2001) and with solid-state NMR experiments (Hu et al., 1998). Thus the striking variations of the $R_{D,H}$ rates between A–U and G–C pairs must be due to significant differences between the chemical shift anisotropies of the imino protons belonging to uridine and guanidine, at least when they are involved in hydrogen bonds. In fact, the $R_{D,H}$ rates of A–U pairs are so low that we could not measure them accurately (Figure 9).

These results suggest that relatively small differences in the environment could have a significant effect on the proton CSA tensors. This has indeed been predicted by calculations (Czernek, 2001) for imino protons that are *not* involved in hydrogen bonds. For imino protons of uracil, $\delta_{11} \approx \delta_{22} \neq \delta_{33}$, with a unique axis that lies parallel to the r_{DH} vector. For imino protons of guanine on the other hand, calcula-

Table 2. Principal components δ_{ii} of the imino proton CSA tensors obtained by least-squares fitting (assuming $\alpha_H = 0$) to the measured rates $R_{H,A}$ and $R_{D,H}$ shown in Figure 9. For comparison, the tensors predicted by Czernek (2001) by ab-initio calculations for imino protons with or without hydrogen bonds are also given, transformed to our chemical shift scale through the relationship $\delta_{ii} = 31.3$ ppm $- \sigma_{ii}$. The isotropic chemical shifts $\delta_{iso} = (\delta_{11} + \delta_{22} + \delta_{33})/3$ were kept fixed, so that the number of parameters to be fitted was reduced to two. In brackets: $\Delta\delta_{ii} = \delta_{ii} - \delta_{iso}$. Note that the components obtained in this work are not ordered as usual according to their magnitude (i.e., $\delta_{11} > \delta_{22} > \delta_{33}$) but according to the orientations shown in Figure 2, to facilitate comparison with theoretical predictions

	G–C		
	This work	Czernek, with H bond	Czernek, without H bond
δ_{11} [ppm]	7.2 (−5.2)	27.6 (+13.1)	12.0 (+4.1)
δ_{22} [ppm]	13.2 (+0.8)	14.1 (−0.4)	6.6 (−1.3)
δ_{33} [ppm]	16.8 (+4.4)	1.8 (−12.7)	5.0 (−2.9)
δ_{iso} [ppm]	12.4	14.5	7.9
α_H [deg]	0	0	0
	A–U		
	This work	Czernek, with H bond	Czernek, without H bond
δ_{11} [ppm]	9.3 (−4.4)	30.9 (+13.6)	11.4 (+2.6)
δ_{22} [ppm]	28.3 (+14.6)	18.9 (+1.6)	9.0 (+0.2)
δ_{33} [ppm]	3.4 (−10.3)	2.0 (−15.3)	5.8 (−3.0)
δ_{iso} [ppm]	13.7	17.3	8.8
α_H [deg]	0	0	0

tions show that $\delta_{11} \neq \delta_{22} \approx \delta_{33}$ with a unique axis that lies perpendicular to the base plane.

The above considerations (and the conclusions about imino proton CSA tensors discussed below) are only valid if there are no CSM/CSM contributions to $R_{D,H}$ and $R_{H,A}$ due to conformational exchange. We don't see any significant CSM/CSM contribution to $R_{D,A}$ (see above) nor any R_{ex} contribution to the single-quantum autorelaxation rate R_2 of the donor nitrogen by CPMG measurements (data not shown), and one expects the same behavior for $R_{D,H}$ and $R_{H,A}$.

We have calculated the rates $R_{D,H}$ and $R_{H,A}$ using calculated CSA tensors of the imino protons (Czernek, 2001) (Table 2) and the (presumably more reliable) nitrogen CSA tensors (Table 1) as discussed above. In contrast to the good fits obtained for the $R_{D,A}$ rates of Figure 7, the calculated rates $R_{D,H}$ and $R_{H,A}$ are not consistent with the experimental rates of Figure 9. The calculated rates (not plotted in Figure 9) are up to four times larger than the experimental rates.

We have therefore attempted to adjust the eigenvalues (principal values) of the imino proton chemical shift anisotropies to fit our measured rates while maintaining the orientations of the tensors of Czernek (2001), i.e., $\alpha_H = 0°$ (see Figure 2), using both measured rates $R_{D,H}$ and $R_{H,A}$ for each base-pair. The presence of two A–U and four G–C pairs with different base plane orientations provides additional information (the intermolecular base-pair G11-C10 was excluded from this fitting procedure). Since the isotropic chemical shift $\delta_{iso} = \frac{1}{3}(\delta_{11} + \delta_{22} + \delta_{33})$ is known, only two parameters, e.g. δ_{11} and δ_{22}, were allowed to be varied for each base pair type. The resulting tensor components are given in Table 2 and compared with calculated values (Czernek, 2001) for imino protons with or without hydrogen bonds. Note that we did not renumber the components according to their magnitude, to facilitate comparison with Czernek's work. The rates $R_{D,H}$ and $R_{H,A}$ calculated with our tensors are shown in Figure 9. Our estimates of the imino proton CSA's are much smaller than those of Czernek. For G–C pairs, the sign of the shielding is even inverted with respect to the *ab initio* calculations. Our δ_{33} components, which are parallel to the r_{DH} vector, are the most deshielded, while Czernek's most deshielded component δ_{11} lies perpendicular to the plane. Our δ_{22} is close to δ_{33}, so that we have a nearly axially symmetric tensor with a unique axis δ_{11}. For A–U base pairs, the situation is completely differ-

ent: the unique component δ_{22} is the most deshielded component.

Conclusions

Four experiments, including two novel methods, have been used to measure various cross-correlation rates in an RNA kissing complex. The reliability of experiments A and B was confirmed by calculations of cross-correlation rates using CSA tensors, geometrical and dynamical properties which have been independently determined experimentally and theoretically in other laboratories or by ourselves. The stem of the kissing complex, which features neither base-pair mismatches nor exchange processes, proves to be a suitable system to test these methods. Surprisingly, the *inter*molecular base pair does not show any significant differences with respect to the stem, which implies that the CSA tensors, geometrical properties and dynamic behavior are the same for *intra*molecular and *inter*molecular base pairs. The experiments C and D measure cross-correlation rates which depend on the CSA tensors of the imino protons. These tensors have never been determined experimentally so far. We made a preliminary attempt to deduce these tensors from our relaxation rates. Comparison with the imino proton tensors calculated by Czernek (2001) by means of DFT shows substantial discrepancies which remain to be explained. There are striking differences in the $R_{D,H}$ and $R_{H,A}$ rates between the two types of base pairs A–U and G–C, which seem to be due to differences between the imino proton CSA tensors, although it cannot be excluded that these are due in part to internal dynamics.

Acknowledgements

We are grateful to Ignacio Tinoco Jr. (Berkeley) for his kind cooperation, to Jiří Czernek for valuable comments on his work, to Elisabetta Chiarparin, Simon Rüdisser and Sapna Ravindranathan for helpful discussions, and to Martial Rey for technical support. We are indebted to the Fonds National de la Recherche Scientifique (FNRS, Switzerland), to the Commission pour la Technologie et l'Innovation (CTI, Switzerland), to the Centre National de la Recherche Scientifique (CNRS, France), and to the European Union (contract HPRN-CT-2000-00092).

References

Akke, M., Fiala, R., Patel, D. and Palmer III, A.G. (1997) *RNA*, **3**, 702–709.

Anderson-Altmann, K.L., Phung, C.G., Mavromoustakis, S., Zheng, Z., Facelli, J.C., Poulter, C.D. and Grant, D.M. (1995) *J. Phys. Chem.*, **99**, 10454–10458.

Anil Kumar, Christy Rani Grace, R. and Madhu, P.K. (2000) *Prog. NMR Spectrosc.*, **37**, 191–319.

Boisbouvier, J., Brutscher, B., Simorre, J.-P. and Marion, P. (1999) *J. Biomol. NMR*, **14**, 241–252.

Brutscher, B., Skrynnikov, N.R., Bremi, T., Brüschweiler, R. and Ernst, R.R. (1997) *J. Magn. Reson.*, **130**, 346–351.

Chiarparin, E., Pelupessy, P., Ghose, R. and Bodenhausen, G. (1999) *J. Am. Chem. Soc.*, **121**, 6876–6883.

Chiarparin, E., Rüdisser, S. and Bodenhausen, G. (2001) *ChemPhysChem.*, **1**, 41–45.

Czernek, J. (2001) *J. Phys. Chem. A*, **105**, 1357–1365.

Czernek, J., Fiala, R. and Sklenár, V. (2000) *J. Magn. Reson.*, **145**, 142–146.

Daragan, V.A. and Mayo, K.H. (1997) *Prog. NMR Spectrosc.*, **31**, 63–105.

Dayie, K.T., Brodsky, A.S. and Williamson, J.R. (2002) *J. Mol. Biol.*, **317**, 263–278.

De Tapia, M., Metzler, V., Mougel, M., Ehresmann, B. and Ehresmann, C. (1998) *Biochemistry*, **37**, 6077–6085.

Dingley, A.J. and Grzesiek, S. (1998) *J. Am. Chem. Soc.*, **120**, 8293–8297.

Emsley, L. and Bodenhausen, G. (1990) *Chem. Phys. Lett.*, **168**, 297–303.

Felli, I., Richter, C., Griesinger, C. and Schwalbe, H. (1999) *J. Am. Chem. Soc.*, **121**, 1956–1957.

Frueh, D. (2002) *Prog. NMR Spectrosc.*, **41**, 305–324.

Früh, D., Tolman, J.R., Bodenhausen, G. and Zwahlen, C. (2001) *J. Am. Chem. Soc.*, **123**, 4810–4816.

Geen, H. and Freeman, R. (1991) *J. Magn. Reson.*, **93**, 93–141.

Goldman, M. (1984) *J. Magn. Reson.*, **60**, 437–452.

Griesinger, C. and Ernst, R.R. (1988) *Chem. Phys. Lett.* **152**, 239–247.

Grzesiek, S. and Bax, A. (1993) *J. Am. Chem. Soc.*, **115**, 12593–12594.

Hall, K.B. and Tang, C. (1998) *Biochemistry*, **37**, 9323–9332.

Hu, J.Z., Facelli, J.C, Alderman, D.W., Pugmire, R.J. and Grant, D.M. (1998) *J. Am. Chem. Soc.*, **120**, 9863–9869.

Kim, C.-H. and Tinoco Jr., I. (2000) *Proc. Natl. Acad. Sci. USA*, **97**, 9396–9401.

Kupce, E., Boyd, J. and Campbell, I.D. (1995) *J. Magn. Reson. B*, **106**, 300–303.

Lipari, G. and Szabo, A. (1982) *J. Am. Chem. Soc.*, **104**, 4546–4559.

Markley, J.L., Bax, A., Arata, Y., Hilbers, C.W., Kaptein, R., Sykes, B.D., Wright, P.E. and Wüthrich, K. (1998) *J. Mol. Biol.*, **280**, 933–952.

Peng, J.W. and Wagner, G. (1994) *Meth. Enzymol.*, **239**, 563–595.

Pervushin, K. (2001) *J. Biomol. NMR*, **20**, 275–285.

Pervushin, K., Ono, A., Fernández, C., Szyperski, T., Kainosho, M. and Wüthrich, K. (1998) *Proc. Natl. Acad. Sci. USA*, **95**, 14147–14151.

Piotto, M., Saudek, V. and Sklenár, V. (1992) *J. Biomol. NMR*, **2**, 661–665.

Press, W.H., Flannery, B.P., Teukolsky, S.A and Vetterling, W.T. (1986) *Numerical Recipes*, Cambridge University Press, Cambridge, New York.

Reif, B., Diener, A., Hennig, M., Maurer, M. and Griesinger, C. (2000) *J. Magn. Reson.*, **143**, 45–68.

Richter, C., Griesinger, C., Felli, I., Cole, P.T., Varani, G. and Schwalbe, H. (1999) *J. Biomol. NMR*, **15**, 241–250.
Richter, C., Reif, B., Griesinger, C. and Schwalbe, H. (2000) *J. Am. Chem. Soc.*, **122**, 12728–12731.
Riek, R. (2001) *J. Magn. Reson.*, **149**, 149–153.
Rüdisser, S. and Tinoco Jr., I. (2000) *J. Mol. Biol.*, **295**, 1211–1223.
Schwalbe, H., Carlomagno, T., Hennig, M., Junker, J., Reif, B., Richter, C. and Griesinger, C. (2001) *Meth. Enzymol.*, **338**, 35–81.
Werbelow, L.G. and Grant, D.M. (1977) *Adv. Magn. Reson.*, **9**, 189–299.
Yang, D., Konrat, R. and Kay, L.E. (1997) *J. Am. Chem. Soc.*, **119**, 11938–11940.